Floquet Topological Phases Driven by $\mathcal{PT}$ Symmetric Nonunitary Time Evolution

Dakyeong Kim,[1] Ken Mochizuki,[1] Norio Kawakami,[2] and Hideaki Obuse[1]

[1] *Department of Applied Physics, Hokkaido University, Sapporo 060-8628, Japan*
[2] *Department of Physics, Kyoto University, Kyoto 606-8502, Japan*

(ΩDated: September 30, 2016)

We study Floquet topological phases driven by $\mathcal{PT}$ symmetric nonunitary time evolution in one dimension, based on an experimental setup of discrete-time quantum walks. We develop, for nonunitary time-evolution operators, a procedure to calculate topological invariants for Floquet topological phases and find that the bulk-edge correspondence gives correct predictions of the emergent edge states. These edge states make exponential growth of wavefunction amplitudes at specific positions with time controllable. Hereby, we propose that these phenomena inherent in open quantum systems are feasibly observed by present experiments of quantum walks in both classical and quantum regimes.

arXiv:1609.09650v1 [cond-mat.mes-hall] 30 Sep 2016

Introduction: Understanding and controlling open quantum systems are a fundamentally important problem to be solved. A combined parity and time-reversal symmetry, called $\mathcal{PT}$ symmetry, in a non-Hermitian Hamiltonian sheds light on the issue by providing unique and relatively easier solutions, namely, keeping real eigenenegy even in non-Hermitian systems[1, 2]. Accordingly, non-Hermitian systems with $\mathcal{PT}$ symmetry have attracted great attention from various fields in physics, since these systems provide not only further understanding of open quantum systems[3–6] but also novel applications[7–16] which cannot be realized by closed Hermitian systems.

Motivated by these remarkable developments in $\mathcal{PT}$ symmetry of time-independent non-Hermitian Hamiltonians, $\mathcal{PT}$ symmetry for time-dependent systems described by a time-evolution operator is also investigated[17–23], but it is relatively less well understood because of difficulty even in identifying $\mathcal{PT}$ symmetry for the nonunitary operator associated with a time-dependent Hamiltonian. Recently, it is clarified in Refs. [24, 25] that not only $\mathcal{PT}$ symmetry but also additional symmetries can be facilely defined for the nonunitary operator by focusing on discrete-time quantum walks(QWs)[26, 27]. Remarkably, the nonunitary QW with gain and loss has been realized in experiments by implementing optical fiber loops[28].

Taking account of facility in maintaining symmetries of nonunitary operators, the QW is also an ideal platform to study Floquet topological phases(FTPs) of nonunitary time-evolution operators, since symmetries are also very important for topological insulators. While topological insulators have novel surface states protected by symmetries, materials which possess nontrivial topological phases are limited. Therefore, approaches to artificially induce nontrivial topological phases are becoming important. One possible way is FTPs which are induced by applying external fields to a topologically trivial system so that the time-evolution operator possesses topologically non-trivial phases[29–37]. FTPs of unitary QWs has been intensively studied theoretically[38–46]. Furthermore, edge states associated with FTPs are observed in experiments for one[47, 48] and two[49] dimensional systems. It is remarkable that these experiments are performed in optical systems. Since loss of photons or light is unavoidable in optical systems, effects of dissipation (and gain in some setups in like Ref. [28]) on FTPs should be investigated. It is worth mentioning that while topological phases of time-independent non-Hermitian Hamiltonians with $\mathcal{PT}$ symmetry are studied in Refs. [50] and [51] and there are several developments [52–57] in the last couple of years, FTPs for time-dependent non-Hermitian systems, *i.e.* nonunitary time-evolution operators, have not yet been studied.

In this Letter, we study FTPs and the corresponding edge states of the $\mathcal{PT}$ symmetric nonunitary QW with gain and loss in one dimension(1D), whose setup is based on the experiment in Ref. [28]. We develop a procedure to calculate topological invariants for FTPs driven by nonunitary time-evolution and show that the emergent edge states satisfy the bulk-edge correspondence. We demonstrate that these edge states contribute to exponential amplification of wavefunction amplitudes at specific positions with time. Accordingly, we propose that these phenomena inherent in $\mathcal{PT}$ symmetric nonunitary dynamics are feasibly observed by current experimental setups of quantum walks implemented by not only classical coherent lights[28] but also single photons in the quantum regime[47, 58, 59].

Model: Here, we introduce the time-evolution operator of the 1D nonunitary QW realized in the experiment in Ref. [28] and studied further in Ref. [24]. The basis of the walker is defined from two internal states, $|L\rangle := (1,0)^T$ and $|R\rangle := (0,1)^T$ and 1D position space $|n\rangle$, where $n \in \mathbb{Z}$. Thereby, the wavefunction at time step t, $|\psi(t)\rangle$, is written as $|\psi(t)\rangle = \sum_{n\in\mathbb{Z}} \sum_{s=L,R} \psi_{n,s}(t)|n\rangle \otimes |s\rangle$. The time-evolution operator U for one time step of the 1D nonunitary QW is defined by the product of elemental operators:

$$U := S\,G\,C(\theta_2)\,S\,G^{-1}\,C(\theta_1), \tag{1}$$

where each elemental operator is defined as

$$C(\theta_{i=1,2}) := \sum_n |n\rangle\langle n| \otimes \tilde{C}[\theta_i(n)],$$
$$\tilde{C}[\theta_i(n)] := \begin{pmatrix} \cos[\theta_i(n)] & i\sin[\theta_i(n)] \\ i\sin[\theta_i(n)] & \cos[\theta_i(n)] \end{pmatrix} = e^{i\theta_i(n)\sigma_1},$$
$$S := \sum_n |n-1\rangle\langle n| \otimes |L\rangle\langle L| + \sum_n |n+1\rangle\langle n| \otimes |R\rangle\langle R|,$$
$$G := \sum_n |n\rangle\langle n| \otimes \tilde{G}, \qquad \tilde{G} := \begin{pmatrix} e^{\gamma} & 0 \\ 0 & e^{-\gamma} \end{pmatrix} = e^{\gamma\sigma_3}.$$

Here, σ_i $(i = 1, 2, 3)$ are Pauli matrices. The coin operator $C(\theta_i)$ changes the internal states of walkers through the position dependent $\theta_i(n)$ and the shift operator S shifts a walker to its adjacent site depending on its internal state. The gain and loss operator G with positive γ amplifies (dumps) the wavefunction amplitude with the internal state $|L\rangle$ ($|R\rangle$) by the factor e^{γ} ($e^{-\gamma}$), and G^{-1} vice versa.

The wave function after time t is described by

$$|\psi(t)\rangle = U^t|\psi(0)\rangle. \tag{2}$$

The quasienergy ε is defined from the eigen equation of the time-evolution operator:

$$U|\psi_\lambda\rangle = \lambda|\psi_\lambda\rangle, \quad \lambda = e^{-i\varepsilon}. \tag{3}$$

When $\gamma \neq 0$, U becomes nonunitary and $|\lambda| \neq 1$, which makes the quasienergy ε complex, in general. However, if the time-evolution operator possesses $\mathcal{PT}$ symmetry and the eigenstate $|\psi_\lambda\rangle$ is also the eigenstate of the $\mathcal{PT}$ symmetry operator, ε becomes real[2].

Symmetry: It is shown in Ref. [24] that the nonunitary time-evolution operator U in Eq. (1) has various symmetries. Here we briefly summarize relevant symmetries which are important to argue topological phases. As proposed in Ref. [42], we need to apply the symmetry time frame to the time-evolution operator when we argue symmetry of time-evolution operators. In the present case, the time-evolution operator fitted in the symmetry time frame reads

$$U' = C\left(\theta_1/2\right) G\, S\, C(\theta_2)\, S\, G^{-1}\, C\left(\theta_1/2\right). \tag{4}$$

$\mathcal{PT}$ symmetry requires the time-evolution operator to satisfy $(\mathcal{PT})U'(\mathcal{PT})^{-1} = U'^{-1}$. This relation is satisfied by using the $\mathcal{PT}$ symmetry operator $\mathcal{PT} = \sum_n |-n\rangle\langle n| \otimes \sigma_0 \mathcal{K}$, where $\mathcal{K}$ and σ_0 are complex conjugation and an identity matrix $\mathbb{I}_2$ respectively, and with a constraint on position dependences of $\theta_{i=1,2}(n)$:

$$\theta_i(n) = \theta_i(-n). \tag{5}$$

The time-evolution operator U' also retains parity-chiral symmetry(PCS), which is combined symmetry of parity and chiral symmetries in the same fashion with $\mathcal{PT}$ symmetry, $(\mathcal{P\Gamma})U'(\mathcal{P\Gamma})^{-1} = U'^{-1}$, with the symmetry operator $\mathcal{P\Gamma} = \sum_n |-n\rangle\langle n| \otimes \sigma_3$. By combining $\mathcal{PT}$ symmetry and PCS operators, particle-hole symmetry $\mathcal{C}U'\mathcal{C}^{-1} = U'$ is established with $\mathcal{C} = \sum_n |n\rangle\langle n| \otimes \sigma_3\mathcal{K}$.

Floquet topological phases: It is worth mentioning that, when $\gamma = 0$, the time-evolution operator U recovers time-reversal and chiral symmetries. Thereby, the system with $\gamma = 0$ is classified in class BDI in the AZ classification and possibly possesses non-trivial topological phases[60]. In Ref. [42], it is shown that the unitary QW belonging to class BDI possesses two topological numbers ν_0 and ν_π for quasienergy gaps around $\varepsilon = 0$ and π, respectively, due to 2π periodicity of the quasienergy. While, for finite γ, time-reversal and chiral symmetries are broken, $\mathcal{PT}$ and parity-chiral symmetries possess the similar properties with the original symmetries. Since topological numbers are believed to be robust against perturbations which preserve symmetries, it is of particular interest to study FTPs and associated edge states of the nonunitary QW with gain and loss in Eq. (1).

At first, we clarify a condition for finding finite band gaps of the quasienergy around $\varepsilon = 0$ and π, so that topological numbers are well defined. By assuming a homogeneous system, *i.e.* $\theta_1(n)$ and $\theta_2(n)$ are constant, we rewrite the time-evolution operator U' to $U'(k)$ in momentum space by the Fourier transformation:

$$U'(k) = \sum_{i=0,1,2,3} d_i(k)\sigma_i, \tag{6}$$
$$d_0(k) = \cos\theta_1\cos\theta_2\cos(2k) - \sin\theta_1\sin\theta_2\cosh(2\gamma),$$
$$d_1(k) = \sin\theta_1\cos\theta_2\cos(2k) + \cos\theta_1\sin\theta_2\cosh(2\gamma),$$
$$d_2(k) = d_2 = -\sin\theta_1\sinh(2\gamma), \quad d_3(k) = \cos\theta_2\sin(2k),$$

which satisfies $\sum_{i=0,1,3} d_i^2(k) - d_2^2 = 1$. Then, the eigenvalue of $U'(k)$ is derived as $\lambda_\pm(k) = d_0(k) \pm i\sqrt{1 - d_0^2(k)}$. On one hand, when $|d_0(k)| \leq 1$ for any $k \in [0, 2\pi)$, the quasienergy ε is kept to be real because $|\lambda_\pm| = 1$, although U' is nonunitary. On the other hand, when $|d_0(k)| > 1$ at a certain range of k, the eigenvalue takes only the real value, $\lambda_\pm = d_0(k) \mp \sqrt{d_0^2(k) - 1} (\neq \pm 1)$, and then the quasienergy ε becomes complex. The former and latter situations are called an unbroken $\mathcal{PT}$ symmetry phase and a broken $\mathcal{PT}$ symmetry phase, respectively[2]. Remarkably, the condition of the presence or absence of the quasienergy band gap around $\varepsilon = 0$ or π , *i.e.* $\lambda = \pm 1$, is also discerned by the above unbroken/broken $\mathcal{PT}$ symmetry phases. Thereby, the condition $|d_0(k = n\pi/2)| = 1$, where n is an integer, gives phase boundaries of topological numbers as shown in Fig. 1, and we focus on unbroken $\mathcal{PT}$ symmetry phases hereafter. We note that, for the nonunitary QW, the parameter space where topological numbers are not well defined extends in finite regions, while it features lines for the unitary QW ($\gamma = 0$)[46].

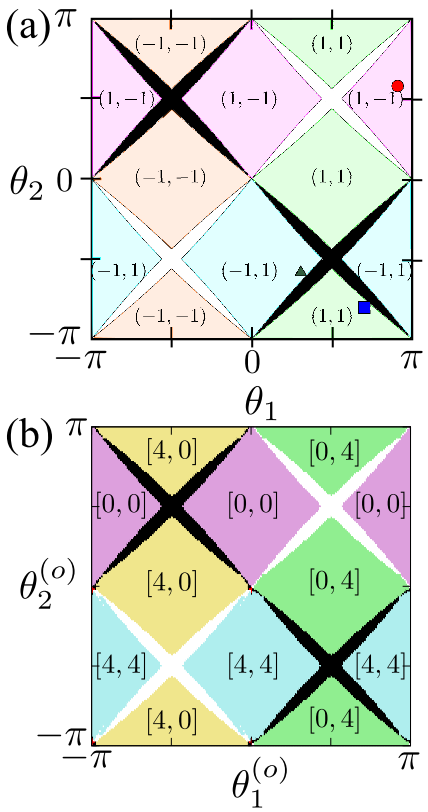

FIG. 1. (Color online)(a) The phase diagram of topological numbers (ν_0, ν_π) as functions of θ_1 and θ_2 of the nonunitary quantum walk in Eq. (1) with $e^\gamma = 1.1$. The regions with topological numbers (ν_0, ν_π) correspond to unbroken $\mathcal{PT}$ symmetry phases, while black and white regions represent broken $\mathcal{PT}$ symmetry phases with complex eigenenergies whose real parts are $\mathrm{Re}(\varepsilon) = 0$ and π, respectively. The circle represents $(\theta_1^{(i)}, \theta_2^{(i)}) = (9\pi/10, 3\pi/5)$, while rectangle and triangle represent $(\theta_1^{(o)}, \theta_2^{(o)}) = (7\pi/10, -4\pi/5)$ (case A), and $(3\pi/10, -3\pi/5)$ (case B), respectively, which are used in numerical verifications in Fig. 3. (b) The number of edge states $[N_0, N_\pi]$ appearing at the quasienergy $\mathrm{Re}(\varepsilon) = 0, \pi$ in the system in Eq. (10) with parameters in Eq. (11), for various values of $\theta_1^{(o)}$ and $\theta_2^{(o)}$.

Next, we develop a procedure to calculate topological numbers of the nonunitary QW by generalizing a procedure for unitary QWs belonging to class BDI developed in Ref. [42] to nonunitary QWs with $\mathcal{PT}$ symmetry and PCS. At first, we define topological numbers of the nonunitary time-evolution operator $U'(k)$ from Zak phases in open quantum systems by using the biorthogonal basis [in other words, right and left eigenstates of $U'(k)$], $|\psi(k)\rangle$ and $\langle\chi(k)|$[61]. We derive the Zak phase

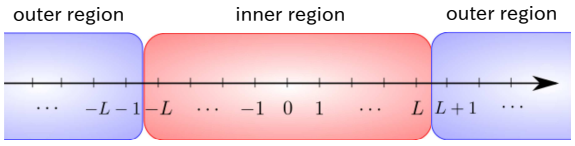

FIG. 2. (Color online)The schematic view of the $\mathcal{PT}$ symmetric nonunitary QW defined in Eq. (10).

φ'_Z as follows[62]

$$\varphi'_Z = -i \oint \langle\chi(k)|\frac{d}{dk}|\psi(k)\rangle dk = -\frac{1}{2}\oint d\vartheta_k \mp \frac{i}{2}\oint \tan 2\Omega_k \frac{d\vartheta_k}{dk} dk. \quad (7)$$

where

$$|d(k)|e^{i\vartheta_k} = d_3(k) + id_1(k),$$
$$\cos(2\Omega_k) = \sqrt{1 - \left(\frac{d_2}{|d(k)|}\right)}, \quad \sin(2\Omega_k) = \frac{d_2}{|d(k)|}.$$

Since the Zak phase φ'_Z defined in Eq. (7) becomes complex in general, we define the topological number ν' with the assumption that only the real part of Zak phases is relevant for the topological number

$$\nu' = \pi^{-1}\mathrm{Re}(\varphi'_Z). \quad (8)$$

As shown in Ref. [42], since ν' does not contain enough information to characterize two topological numbers for quasienergy $\varepsilon = 0$ and π, we need to treat the other time-evolution operator fitted in the different symmetry time frame. In the case of the nonunitary QW with PCS, we can also find the other time-evolution operator $U'' = C(\theta_2/2)\, S\, G^{-1}\, C(\theta_1)\, G\, S\, C(\theta_2/2)$, which has the same symmetries with U'. We calculate ν'' from the time-evolution operator U'' in the same way with ν'. Finally, we apply the formula to calculate topological numbers ν_0 and ν_π for edge states at $\varepsilon = 0$ and π, respectively, derived in Ref. [42] from ν' and ν'' for nonunitary QWs with $\mathcal{PT}$ symmetry and PCS:

$$\nu_0 = \frac{\nu' + \nu''}{2}, \qquad \nu_\pi = \frac{\nu' - \nu''}{2}. \quad (9)$$

Taking Eqs. (7)-(9) into account, we derive topological numbers (ν_0, ν_π) of the nonunitary time-evolution operator U with $e^\gamma = 1.1$[62]. The result is shown in the phase diagram in Fig. 1. We note that the topological numbers for the nonunitary QW defined in Eq. (8) are the same with those for the unitary QW ($\gamma = 0$) unless both two band gaps around $\varepsilon = 0$ and π are open. Therefore, the topological numbers are robust against gain and loss of the $\mathcal{PT}$ symmetric non-unitary driving.

Bulk-edge correspondence: Having established the phase diagram, we study whether the bulk-edge correspondence gives the correct number of edge states even

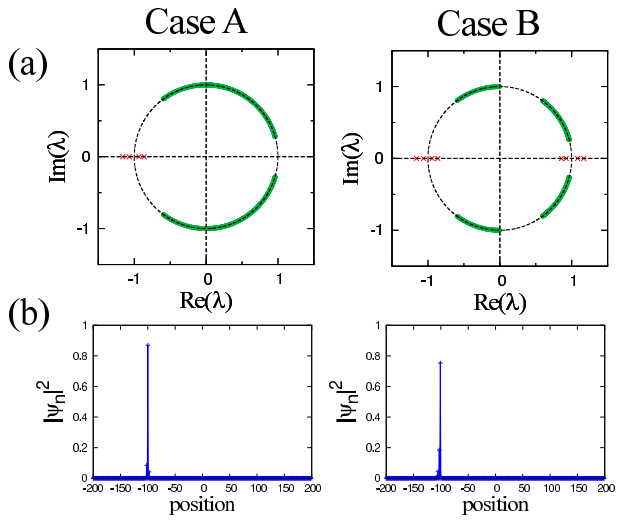

FIG. 3. (Color online) The eigenvalue λ of the time-evolution operator on the complex plane with $\theta_1^{(o)}$ and $\theta_2^{(o)}$ for the case A (left) and B(right). The red crosses in each figure represent eigenvalues of edge states. (b) The probability distribution $|\Psi_n|^2 = \sum_{s=L,R} |\psi_{\lambda,n,s}|^2$ of one of eigenvectors, $|\psi_\lambda\rangle = \sum_{n,s=L,R} \psi_{\lambda,n,s}|n\rangle \otimes |s\rangle$, corresponding to edge states localizing near the interface $L = -100$ for the case A and B.

for the FTP driven by $\mathcal{PT}$ symmetric non-unitary time evolution. In order to induce edge states, we need to spatially change topological numbers by introducing position dependent angles $\theta_{i=1,2}$ of the coin operators under the condition in Eq. (5). Accordingly, the system is separated into three, an inner and two outer regions as shown in Fig. 2, which are discerned by the value of θ_1 and θ_2:

$$\theta_{1(2)}(n) = \begin{cases} \theta_{1(2)}^{(o)} & (n \le -L-1)\,, \\ \theta_{1(2)}^{(i)} & (-L \le n \le L)\,, \\ \theta_{1(2)}^{(o)} & (n \ge L+1)\,. \end{cases} \tag{10}$$

Note that there are two interfaces near $n = \pm L$ where the topological number varies from one value to the other, in contrast to the normal setup to induce edge states of unitary QWs where symmetries require no spatial constraints on $\theta_i(n)$. In the following numerical simulations, we fix parameters

$$e^\gamma = 1.1 \quad \text{and} \quad (\theta_1^{(i)}, \theta_2^{(i)}) = (9\pi/10, 3\pi/5). \tag{11}$$

When we calculate eigenvalues of the time-evolution operator U by numerical diagonalizations, the periodic boundary conditions are imposed on two ends of the finite system of $-M \le n \le M-1$ with $M = 2L = 200$. First, in Fig. 3(a), we show the eigenvalues of the time-evolution operator for the system in Eq. (10) with fixed $\theta_{1,2}^{(i)}$ and two kinds of $\theta_{1,2}^{(o)}$, which are indicated by symbols in Fig. 1(a). We call systems with $(\theta_1^{(o)}, \theta_2^{(o)}) = (7\pi/10, -4\pi/5)$ and $(3\pi/10, -3\pi/5)$ the case A and B, respectively. According to the phase diagram of topological numbers in Fig. 1(a) with Eq. (11), we expect the existence of two edge states at $\varepsilon = \pi$ near each interface in the case A by the bulk-edge correspondence, while two pairs of two edge states appear at $\varepsilon = 0$ and π near each interface in the case B. The results of numerical diagonalizations are shown in Fig. 3(a). While most of eigenvalues are on the unit circle in the complex plane, we find that there appear four eigenvalues deviating from the circle with $\mathrm{Re}(\varepsilon) = \pi$ in the case A and eight eigenvalues with $|\lambda| \neq 1$ with $\mathrm{Re}(\varepsilon) = 0$ and π in the case B[62]. Since eigenvectors with $|\lambda| \neq 1$ localize near the interface as shown in Fig. 3(b), these states are predicted edge states. Taking into account the fact that the system in Eq. (10) has two interfaces, the numerical results agree with the prediction by the bulk-edge correspondence.

Further we systematically check the above specific result for the whole parameter region of $\theta_{1,2}^{(o)}$ in the following way. We count the number of eigenvectors with $\mathrm{Re}(\varepsilon) = 0, \pi$ for various $\theta_{1,2}^{(o)}$ by treating two different system sizes $M = 80$ and 200. Then, we distinguish edge states from other states (extended states without $\mathcal{PT}$ symmetry due to closing band gaps at $\varepsilon = 0$ or π) by the system size dependence of the number of eigenstates. If the number is unchanged with changing sizes M, the number is recognized as the number of edge states originating from FTPs, N_0 and N_π, with $\mathrm{Re}(\varepsilon) = 0$ and π, respectively. The result is summarized in Fig. 1 (b) showing the set $[N_0, N_\pi]$. Comparing Fig. 1 (a) and (b) in the light of Eq. (11), in unbroken $\mathcal{PT}$ symmetry phases, the number of edge states completely agrees with the prediction by the bulk-edge correspondence. Also, in broken $\mathcal{PT}$ symmetry phases, we observe that the number of eigenstates with $\mathrm{Re}(\varepsilon) = 0, \pi$ increases with increasing the size M, except a few points (shown by red) where the number(≥ 9, in most cases) shows no system size dependence. However, this would be due to finite size effects and could be improved by using larger M. Thereby, we conclude that the bulk-edge correspondence works even for FTPs driven by $\mathcal{PT}$ symmetry nonunitary time evolution. We note, depending on the value of θ in inner and outer regions, eigenstates with $\mathrm{Re}(\varepsilon) \neq 0$ and π may have the complex quasienergy (see Ref. [62] for details).

Dynamics: Finally, we study dynamics of wavefunctions driven by the time-evolution operator U in the case B with $L = 25$ and the initial state $|\psi(0)\rangle = |-4\rangle \otimes |R\rangle$. Here, we introduce the probability to find a walker at site n and time t, $P(n,t) \equiv \sum_{s=L,R} |\psi_{n,s}(t)|^2$. Figure 4(a) demonstrates that the probabilities at two interfaces increase with increasing time, although the initial position is far from the interfaces. This digests peculiar phenomena of the $\mathcal{PT}$ symmetric nonunitary QW, since observation of edge states in unitary QWs requires that the initial state should be very close to the interface[47, 48]. In Fig. 4 (b), we show the probability near the interface

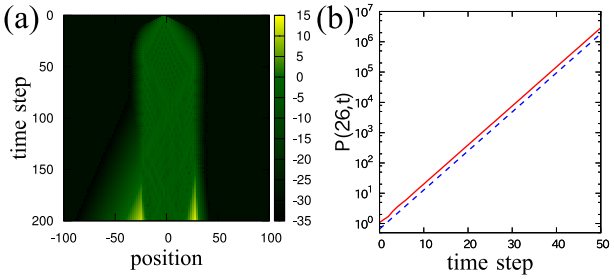

FIG. 4. (Color online) (a) The contour map of $\ln P(n,t)$ in the position and time step plane.(b) The semi-logarithmic plot of time-step dependences of $P(26,t)$ near the interface $L=25$. The dashed line represents Eq. (12) with $\beta \approx \ln(1.16)$.

$P(26,t)$ with $|\psi(0)\rangle = |26\rangle \otimes |R\rangle$ and find that the probability $P(26,t)$ increases exponentially with time. Taking Eqs. (2) and (3) into account, this enhancement of probabilities is the manifestation of edge states with largest $\mathrm{Im}(\varepsilon)$. This is confirmed by the dashed line in Fig. 4 (b) showing

$$P_e(t) \propto \exp(2\beta t), \quad \beta = \max(\mathrm{Im}(\varepsilon)), \tag{12}$$

where β represents a largest value of the imaginary part of the quasienergy.

Discussion and conclusion: We have studied FTPs driven by $\mathcal{PT}$ symmetric nonunitary time evolution realized by the QW. The results investigated here, which are peculiar to $\mathcal{PT}$ symmetric open systems, can be observed from the time-step dependence of probability distributions in the experimental setup in Ref. [28]. Furthermore, although the experiment in Ref. [28] uses classical coherent lasers, it is possible to generalize our theory to passive $\mathcal{PT}$ symmetric systems. Thereby the intrinsically same phenomena could be observed in other setups, such as bulk optics with single photons[47, 59] and optical fiber networks[58], which are in quantum regime. One of important open questions in the present work is how the imaginary part of quasienergy is determined. Understanding this question would involve currently argued issues of open quantum systems such as a better definition of Berry phases[20, 23, 61] and bound states[5, 16]. We leave this for future work.

We thank Y. Asano and K. Yakubo for helpful discussions. This work was supported by a Grant-in-Aid for Scientific Research on Innovative Areas "Topological Materials Science" (JSPS KAKENHI Grant No. JP15H5855 and No. JP16H00975) and also JSPS KAKENHI (Grants No. JP16K17760 and No. JP16K05466).

[1] C. M. Bender and S. Boettcher, Phys. Rev. Lett. **80**, 5243 (1998).
[2] C. M. Bender, Rep. Prog. Phys. **70**, 947 (2007).
[3] C. M. Bender, D. C. Brody, and H. F. Jones, Phys. Rev. Lett. **89**, 270401 (2002).
[4] A. Mostafazadeh, J. Math. Phys. **43**, 205 (2002); *ibid.* **43**, 2814 (2002); *ibid.* **43**, 2814 (2002).
[5] N. Moiseyev, *Non-Hermitian Quantum Mechanis* (Cambridge University Press, Cambridge, 2011).
[6] D. C. Brody, J. Phys. A **47**, 3 (2014).
[7] Z. Lin, H. Ramezani, T. Eichelkraut, T. Kottos, H. Cao, and D. N. Christodoulides, Phys. Rev. Lett. **106**, 213901 (2011).
[8] M. A. Miri, P. LikamWa, and D. N. Christodoulides, Opt. Lett. **37**, 764 (2012).
[9] A. Mostafazadeh, Phys. Rev. A **87**, 012103 (2013).
[10] A. Guo and G. J. Salamo, D. Duchesne, R. Morandotti, M. Volatier-Ravat, V. Aimez, G. A. Siviloglou, D. N. Christodoulides, Phys. Rev. Lett. **103**, 093902 (2009).
[11] C. E. Rüter, K. G. Kakris, R. El-Ganainy, D. N. Christodoulides, M. Mordechai, and D. Kip, Nat. Phys. **6**, 192 (2010).
[12] B. Peng, S. K. Ozdemir, F. Lei, F. Monifi, M. Gianfreda, G. L. Long, S. Fan, F. Nori, C. M. Bender, and L. Yang, Nat. Phys. **10**, 394 (2014).
[13] B. Peng, S. K. Ozdemir, S. Rotter, H. Yilmaz, M. Liertzer, F. Monifi, C. Bender, F. Nori, and L. Yang, Science **346**, 328 (2014).
[14] L. Feng, Z. J. Wong, R-M. Ma, Y. Wang, and X. Zhang, Science **346**, 972 (2014).
[15] H. Hodaei, M-A. Miri, M. Heinrich, D. N. Christodoulides, and M. Khajavikhan, Science **346**, 975 (2014).
[16] S. Garmon, M. Gianfreda, and N. Hatano, Phys. Rev. A **92**, 022125 (2015).
[17] A. Mostafazadeh, Phys. Lett. B **659**, 208 (2007).
[18] N. Moiseyev, Phys. Rev. A **83**, 052125 (2011) .
[19] X. Luo, J. Huang, H. Zhong, X. Qin, Q. Xie, Y. S. Kivshar, C. Lee, Phys. Rev. Lett. **110**, 243902 (2013).
[20] J. Gong and Q. H. Wang, J. Phys. A **46**, 485302 (2013).
[21] Y. N. Joglekar, R. Marathe, P. Durganandini, and R. K. Pathak, Phys. Rev. A **90**, 040101 (2014).
[22] J. Gong and Q. H. Wang, Phys. Rev. A **91**, 042135 (2015).
[23] M. Maamache, Phys. Rev. A **92**, 032106 (2015).
[24] K. Mochizuki, D. Kim, and H. Obuse, Phys. Rev. A **93**, 062116 (2016).
[25] K. Mochizuki and H. Obuse, arXiv:1608.00719.
[26] J. Kempe, Quantum random walks: an introductory overview, Contemp. Phys. **44**, 307 (2003).
[27] A. Ambainis, Quantum walks and their algorithmic applications, Int. J. Quantum Inform. **01**, 507 (2003).
[28] A. Regensburger, C. Bersch, M-A. Miri, G. Onishchukov, D. N. Chistodoulides, and U. Peschel, Nature **488**,167 (2012).
[29] T. Oka and H. Aoki, Phys. Rev. B **79**, 081406(R) (2009).
[30] T. Kitagawa, E. Berg, M. Rudner, and E. Demler, Phys. Rev. B **82**, 235114 (2010).
[31] N. H. Lindner, G. Refael, and V. Galitski, Nat. Phys. **7**, 490 (2011).
[32] J. Cayssol, B. Dóra, F. Simon, and R. Moessner, Phys. Status Solidi RRL **7**, 101 (2013).
[33] M. S. Rudner, N. H. Lindner, E. Berg, and M. Levin, Phys. Rev. X **3**, 031005 (2013).
[34] M. C. Rechtsman, J. M. Zeuner, Y. Plotnik, Y. Lumer, D. Podolsky, F. Dreisow, S. Nolte, M. Segev, and A. Szameit,

Nature (London) **496**, 196 (2013).
[35] Y. Wang, H. Steinberg, P. Jarillo-Herrero, and N. Gedik, Science **342**, 453 (2013).
[36] G. Jotzu, M. Messer, R. Desbuquois, M. Lebrat, T. Uehlinger, D. Greif, and T. Esslinger, Nature (London) **515**, 237 (2014).
[37] M. Aidelsburger, M. Atala, M. Lohse, J. T. Barreiro, B. Paredes, and I. Bloch, Phys. Rev. Lett. **111**, 185301 (2013).
[38] T. Kitagawa, M. S. Rudner, E. Berg, and E. Demler, Phys. Rev. A **82**, 033429 (2010).
[39] T. Kitagawa, Quantum Inf. Process. **11**, 1107 (2012).
[40] H. Obuse and N. Kawakami, Phys. Rev. B **84**, 195139 (2011).
[41] J. K. Asbóth, Phys. Rev. B **86**, 195414 (2012).
[42] J. K. Asbóth and H. Obuse, Phys. Rev. B **88**, 121406 (2013).
[43] B. Tarasinski, J. K. Asbóth, and J. P. Dahlhaus, Phys. Rev. A **89**, 042327 (2014).
[44] J. M. Edge and J. K. Asbóth, Phys. Rev. B **91**, 104202 (2015).
[45] J. K. Asboth and J. M. Edge, Phys. Rev. A **91**, 022324 (2015).
[46] H. Obuse, J. K. Asbóth, Y. Nishimura, and N. Kawakami, Phys. Rev. B **92**, 045424 (2015).
[47] T. Kitagawa, M. A. Broome, A. Fedrizzi, M. S. Rudner, E. Berg, I. Kassal, A. Aspuru-Guzik, E. Demler, and A. G. White, Nat. Commun. **3**, 882 (2012).
[48] S. Barkhofen, T. Nitsche, F. Elster, L. Lorz, A. Gábris, I. Jex, and C. Silberhorn, arXiv:1606.00299.
[49] S. Mukherjee, A. Spracklen, M. Valiente, E. Andersoon, P. Öhberg, N. Goldman, and R. R. Thomson, arXiv:1604.05612.
[50] K. Esaki, M. Sato, K. Hasebe, and M. Kohmoto, Phys. Rev. B **84**, 205128 (2011)
[51] Y. C. Hu and T. L. Hughes, Phys. Rev. B **84**, 153101 (2011).
[52] H. Schomerus, Optics Letters **38**, 1912 (2013).
[53] C. Poli, M. Bellec, U. Kuhl, f. Mortessagne, and H. Schomerus, Nat. Commun. **6**, 6710 (2015)
[54] S. Malzard, C. Poli, and H. Schomerus, Phys. Rev. Lett. **115**, 200402(2015).
[55] T. E. Lee, Phys. Rev. Lett. **116**, 133903 (2016).
[56] C. Yuce, Phys. Rev. A **93**, 062130 (2016).
[57] C. W. Ling, K. H. Choi, T. C. Mlk, Z-Q. Zhang, and K. H. Fung, arXiv:1606.05851 (2016).
[58] A. Schreiber, K. N. Cassemiro, V. Potoček, A. Gábris, P. J. Mosley, E. Andersson, I. Jex, and Ch. Silberhorn, Phys. Rev. Lett. **104**, 050502 (2010).
[59] P. Xue, H. Qin, and B. Tang, Sci. Rep. **4**, 4825 (2014).
[60] A. P. Schnyder, S. Ryu, A. Furusaki, and A. W. W. Ludwig, Phys. Rev. B **78**, 195125 (2008).
[61] J. C. Garrison and E. M. Wright, Phys. Lett. A **128**, 177 (1988).
[62] See details for the supplemental material.

Supplemental Material for "Floquet Topological Phases Driven by $\mathcal{PT}$ Symmetric Nonunitary Time Evolution"

In this supplemental material, we explain details of derivations of Zak phases and the phase diagram of two topological numbers, ν_0 and ν_π, for $\mathcal{PT}$ symmetric nonunitary quantum walks. We also present a detailed analysis on unbroken or broken $\mathcal{PT}$ symmetric phases for all eigenstates.

Calculation of Zak phases of $\mathcal{PT}$ symmetric nonunitary quantum walks

Here, we derive Eq. (7) in the main text. First, we describe the time-evolution operator in momentum space $U'(k)$ in Eq. (6) in the main text using Pauli matrices σ_i $(i = 1, 2, 3)$ and an identity matrix $\sigma_0 = \mathbb{I}_2$:

$$U'(k) = d_0(k)\sigma_0 + id_1(k)\sigma_1 + d_2(k)\sigma_2 + id_3(k)\sigma_3, \tag{S1}$$

$$d_0(k) = \cos\theta_1\cos\theta_2\cos 2k - \sin\theta_1\sin\theta_2\cosh 2\gamma,$$

$$d_1(k) = \sin\theta_1\cos\theta_2\cos 2k + \cos\theta_1\sin\theta_2\cosh 2\gamma, \tag{S2}$$

$$d_2(k) = d_2 = -\sin\theta_2\sinh 2\gamma, \tag{S3}$$

$$d_3(k) = \cos\theta_2\sin 2k, \tag{S4}$$

where a relation $d_0^2(k) + d_1^2(k) - d_2^2 + d_3^2(k) = 1$ is satisfied. In order to simplify the calculation of the Zak phase, we apply a unitary transformation to $U'(k)$ so that the coefficient of σ_3 vanishes when $\gamma = 0$:

$$\begin{aligned} U'_u(k) &= \exp[i\frac{\pi}{4}\sigma_1]U'(k)\exp[-i\frac{\pi}{4}\sigma_1] \\ &= d_0(k)\sigma_0 + id_1(k)\sigma_1 + id_3(k)\sigma_2 - d_2\sigma_3. \end{aligned} \tag{S5}$$

The eigenvalues and the (right and left) eigenvectors of $U'_u(k)$ are

$$\lambda'_\pm(k) = d_0(k) \pm i\sqrt{1 - d_0^2(k)}, \tag{S6}$$

$$|\ \psi_\pm(k)\ \rangle = \frac{1}{\sqrt{2\cos 2\Omega_k}}(e^{\pm i\Omega_k}, \pm ie^{\mp i\Omega_k}e^{-i\vartheta_k})^T, \tag{S7}$$

$$\langle\ \chi_\pm(k)\ | = \frac{1}{\sqrt{2\cos 2\Omega_k}}(e^{\pm i\Omega_k}, \mp ie^{\mp i\Omega_k}e^{i\vartheta_k}), \tag{S8}$$

where ϑ_k and Ω_k are defined as

$$|d(k)|e^{i\vartheta_k} = d_3(k) + id_1(k) \tag{S9}$$

$$\cos 2\Omega_k = \sqrt{1 - \left(\frac{d_2}{|d(k)|}\right)^2}, \quad \sin 2\Omega_k = \frac{d_2}{|d(k)|}. \tag{S10}$$

We calculate the Zak phase in open quantum systems by using the biothogonal basis $|\psi(k)\rangle$ and $\langle\chi(k)|$ in Eqs. (S7) and (S8), respectively,

$$\varphi'_{Z\pm} = -i\oint\langle\chi_\pm(k)|\frac{d}{dk}|\psi_\pm(k)\rangle dk. \tag{S11}$$

The differentiation of the right eigenstate $|\ \psi_\pm(k)\ \rangle$ by the wave number k is given by

$$\begin{aligned} &\frac{d}{dk}|\ \psi_\pm(k)\ \rangle \\ &= \frac{2\sin 2\Omega_k}{(2\cos 2\Omega_k)^{3/2}}\frac{d\Omega_k}{dk}\begin{pmatrix} e^{\pm i\Omega_k} \\ \pm ie^{\mp i\Omega_k}e^{-i\vartheta_k}\end{pmatrix} + \frac{1}{\sqrt{2\cos 2\Omega_k}}\begin{pmatrix} \pm ie^{\pm i\Omega_k}\frac{d\Omega_k}{dk} \\ \pm i(\mp ie^{\mp i\Omega_k}\frac{d\Omega_k}{dk}e^{-i\vartheta_k} - ie^{\mp i\Omega_k}e^{-i\vartheta_k}\frac{d\vartheta_k}{dk})\end{pmatrix} \\ &= \frac{1}{\sqrt{2\cos 2\Omega_k}}\begin{pmatrix} (\tan 2\Omega_k \pm i)e^{\pm i\Omega_k}\frac{d\Omega_k}{dk} \\ \pm i[(\tan 2\Omega_k \mp i)\frac{d\Omega_k}{dk} - i\frac{d\vartheta_k}{dk}]e^{\mp i\Omega_k}e^{-i\vartheta_k}\end{pmatrix}. \end{aligned} \tag{S12}$$

From Eqs. (S8) and (S12), the integrand of Eq. (S11) becomes

$$\begin{aligned}
&\langle\, \chi_\pm(k) \mid \frac{d}{dk} \mid \psi_\pm(k) \,\rangle \\
&= \frac{1}{2\cos 2\Omega_k}[(\tan 2\Omega_k \pm i)e^{\pm 2i\Omega_k}\frac{d\Omega_k}{dk} + \{(\tan 2\Omega_k \mp i)\frac{d\Omega_k}{dk} - i\frac{d\vartheta_k}{dk}\}e^{\mp 2i\Omega_k}] \\
&= \frac{1}{2\cos 2\Omega_k}[\tan 2\Omega_k(e^{\pm 2i\Omega_k} + e^{\mp 2i\Omega_k})\frac{d\Omega_k}{dk} \pm i(e^{\pm 2i\Omega_k} - e^{\mp 2i\Omega_k})\frac{d\Omega_k}{dk} - ie^{\mp 2i\Omega_k}\frac{d\vartheta_k}{dk}] \\
&= \frac{1}{2\cos 2\Omega_k}[\{2\tan 2\Omega_k \cos 2\Omega_k \pm i(\pm 2i\sin 2\Omega_k)\}\frac{d\Omega_k}{dk} - i(\cos 2\Omega_k \mp i\sin 2\Omega_k)\frac{d\vartheta_k}{dk}] \\
&= \frac{1}{2}[(2\tan 2\Omega_k - 2\tan 2\Omega_k)\frac{d\Omega_k}{dk} - i(1 \mp i\tan 2\Omega_k)\frac{d\vartheta_k}{dk}] \\
&= (-\frac{i}{2} \pm \frac{1}{2}\tan 2\Omega_k)\frac{d\vartheta_k}{dk}. \qquad \text{(S13)}
\end{aligned}$$

Substituting Eq. (S13) into Eq. (S11), the Zak phase of the nonunitary time-evolution operator U'_u becomes

$$\varphi'_{Z\pm} = -\frac{1}{2}\oint d\vartheta_k \mp \frac{i}{2}\oint \tan 2\Omega_k \frac{d\vartheta_k}{dk}dk. \qquad \text{(S14)}$$

Derivation of the phase diagram of topological numbers ν_0 and ν_π

In this section, we explain how to derive the phase diagram of topological numbers ν_0 and ν_π for quasienergy $\varepsilon = 0$ and π, respectively, in Fig. 1 (a) in the main text. In the right hand side of Eq. (S14), the first term of the Zak phases calculated from the biothorgonal basis gives a real number since ϑ_k is always real, and the second term gives a pure imaginary number as long as quasienergy gaps around $\varepsilon = 0, \pi$ are open, *i.e.* Ω_k is real. Since topological numbers are well defined when band gaps are open, we consider parameter regions where both band gaps around $\varepsilon = 0$ and $\varepsilon = \pi$ are open. Also, using the assumption written in the main text, we focus only on the real part of the Zak phase,

$$\mathrm{Re}(\varphi'_Z) = -\frac{1}{2}\oint d\vartheta_k. \qquad \text{(S15)}$$

Using the fact that ϑ_k defined in Eq. (S9) is determined by $d_1(k)$ and $d_3(k)$ in Eqs. (S2) and (S4), respectively, we can understand that $\mathrm{Re}(\varphi'_Z)$ takes values $+2\pi$, -2π, or 0, depending on values of θ_1, θ_2, and γ as explained in Fig. S1. Finally, substituting $\mathrm{Re}(\varphi'_Z)$ for various values of θ_1 and θ_2 into Eq. (8), we can obtain the phase diagram of ν' in (θ_1, θ_2) space as shown in Fig. S2(a).

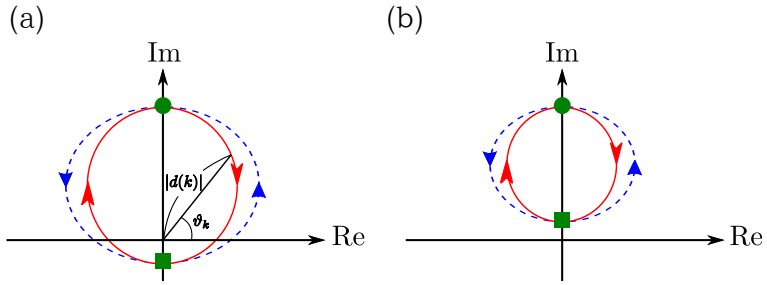

FIG. S1. The schematic view of trajectories of $|d(k)|e^{i\vartheta_k} = d_3(k) + id_1(k)$ as a function of the wave number $k \in [0, 2\pi)$ in complex plane when $d_1(k=0) > 0$ and (a)$|\sin\theta_1 \cos\theta_2| > |\cos\theta_1 \sin\theta_2 \cosh(2\gamma)|$ and (b)$|\sin\theta_1 \cos\theta_2| < |\cos\theta_1 \sin\theta_2 \cosh(2\gamma)|$. The circles and rectangles on the imaginary axis represent the value of $|d(k)|e^{i\vartheta_k}$ when $k = 0$ and $k = \frac{\pi}{2}$, respectively. The arrow on solid (dashed) circle represents the direction of the trajectory of $|d(k)|e^{i\vartheta_k}$ when $\cos\theta_2 > 0$ ($\cos\theta_2 < 0$) as a function of k. When wave number k varies from 0 to 2π, $\mathrm{Re}(\varphi'_Z)$ becomes $+2\pi$ [solid circle in (a)], -2π [dashed circle in (a)], or 0 [in (b)]. In the case $d_1(k=0) < 0$, $\mathrm{Re}(\varphi'_Z)$ can be calculated in the same way.

In order to derive the phase diagram of topological numbers ν_0 and ν_π, we also need to calculate ν''. Comparing $U' = C(\theta_1/2)SGC(\theta_2)G^{-1}SC(\theta_1/2)$ with $U'' = C(\theta_2/2)SG^{-1}C(\theta_1)GSC(\theta_2/2)$, we can immediately obtain ν'' as shown in Fig. S2(b) only by exchanging θ_1 and θ_2 in Fig. S2(a). We note that $d_1(k)$ and $d_3(k)$ are independent of the

sign of γ. Finally, by substituting ν' and ν'' in each parameter region into Eq. (9), we can obtain the phase diagram of ν_0 and ν_π [Fig. 1 (a)].

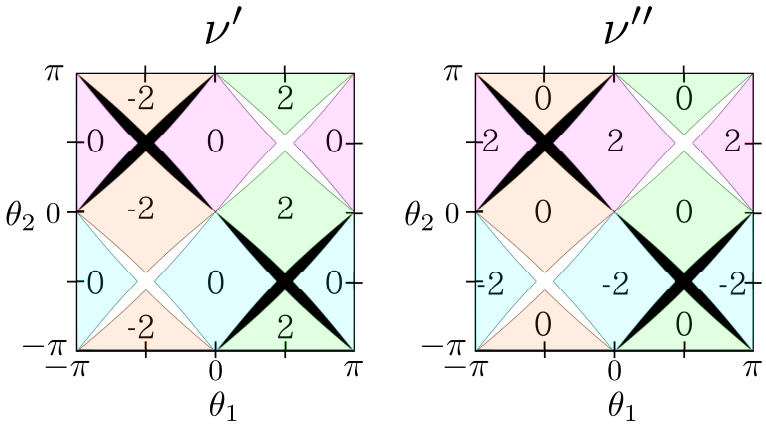

FIG. S2. The value of ν' and ν'' in (θ_1, θ_2) space when $e^\gamma = 1.1$. In the black (white) region, the quasienergy gap around $\varepsilon = 0$ ($\varepsilon = \pi$) is close and ν' and ν'' are not well defined.

Unbroken or broken $\mathcal{PT}$ symmetric phases for all eigenstates

Figure 3 (a) for the cases A and B treated in the main text shows that only edge states with $\mathrm{Re}(\varepsilon) \neq 0$ or π have complex quasienergy, indicating broken $\mathcal{PT}$ symmetry of edge states. However, depending on the value of parameters, other eigenstates with $\mathrm{Re}(\varepsilon) \neq 0$ or π can have complex quasienergy in the inhomogeneous system in Eq. (10) in the main text. Here, we call these states c-states to distinguish from edge states originating from Floquet topological phases and explain details of these numerical results. As we explained, Fig. 1(b) in the main text is obtained from the system size M dependences of the number of eigenstates with $\mathrm{Re}(\varepsilon) = 0$ or π. We repeat the same analysis for all eigenstates and recognize c-states by eigenstates with complex quasienergy with $\mathrm{Re}(\varepsilon) \neq 0$ or π for the system with $M = 200$. The result is shown in Fig. S3.

From Fig. S3, we can understand that c-states exist in wide parameter regions. Figure S4 shows the eigenvalues and probability distributions of c-states when parameters are $\theta_1^{(i)} = \frac{9}{10}\pi$, $\theta_2^{(i)} = \frac{3}{5}\pi$, $\theta_1^{(o)} = -\frac{4}{5}\pi$, $\theta_2^{(o)} = \frac{9}{10}\pi$, and $e^\gamma = 1.1$. As shown in Fig S4, eigenvalues corresponding to c-states shown by red symbols appear not only within a band gap [whose eigenstates are localized near a boundary as shown in Fig. S4 (b)] but also in bulk spectra [whose eigenstates are extended through the system shown in Fig. S4 (c)]. However, we emphasize that imaginary parts of complex quasienergies for edge states originating from Floquet topological phases are generally larger than those for c-states, which we can understand from Fig. S4 (a). Thereby, when we consider the time evolution for the system even with c-states, edge states originating from Floquet topological phases dominate the exponential amplification of probability at the interface.

[1] K. Mochizuki, D. Kim, and H. Obuse, Phys. Rev. A **93**, 062116 (2016).

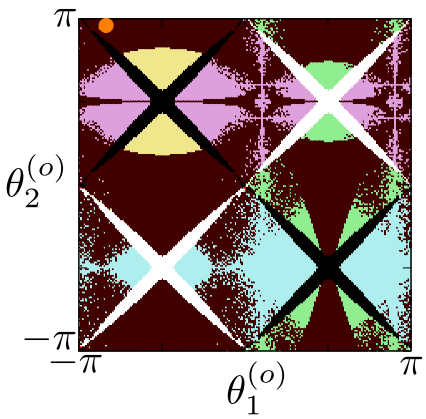

FIG. S3. Existence or absence of c-states and edge states originating to Floquet topological phases at $\mathrm{Re}(\varepsilon) = 0, \pi$. The brown regions represent the existence of c-states for various values of $\theta_1^{(o)}$ and $\theta_2^{(o)}$. The meanings of other colors and values of γ, θ_1^i, and $\theta_2^{(i)}$ are the same as Fig. 1 (b) in the main text. The orange circle represents $(\theta_1^{(o)}, \theta_2^{(o)}) = (-\frac{4}{5}\pi, \frac{9}{10}\pi)$ which is used in the calculation in Fig. S4.

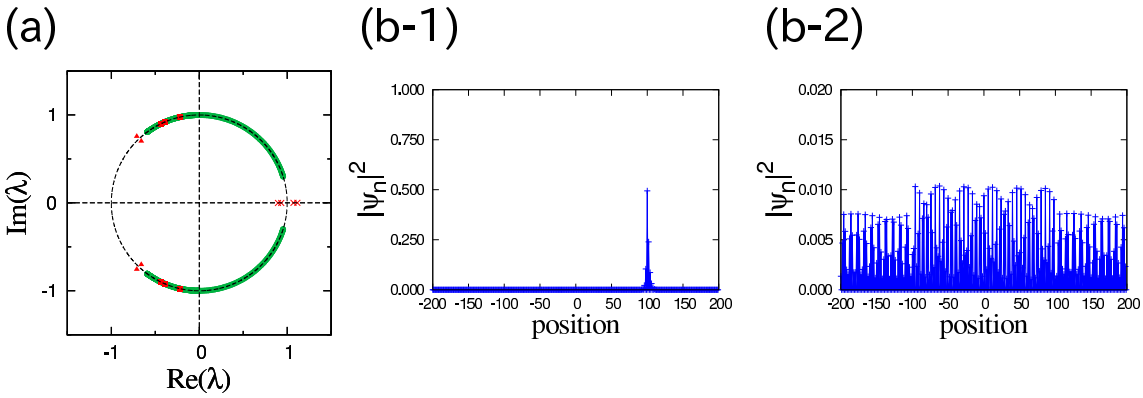

FIG. S4. (a)The eigenvalues and (b) probability distributions of two c-states for the system with the size $M = 200$ and parameters $\theta_1^{(i)} = \frac{9}{10}\pi$, $\theta_2^{(i)} = \frac{3}{5}\pi$, $\theta_1^{(o)} = -\frac{4}{5}\pi$, $\theta_2^{(o)} = \frac{9}{10}\pi$, and $e^{\gamma} = 1.1$. (a)Green dense dots and red symbols (crosses, triangles, and rectangles)) represent the eigenvalues whose absolute value is one and not equal to one (quasienergy is complex), respectively. More precisely, red crosses, triangles, and rectangles correspond to edge states originating from Floquet topological phases, localized c-states inside a band gap, and extended c-states, respectively. (b-1) The probability distribution of one of localized c-states whose eigenvalue corresponds to a red triangle in (a). (b-2) The probability distribution of one of extended c-states whose eigenvalue corresponds to a red rectangle in (a).